AJRCMB Articles in Press. Published on 04-January-2019 as 10.1165/rcmb.2018-0328OC

STAT3 regulates the onset of oxidant-induced senescence in lung fibroblasts

Authors: David W. Waters[1,2], Kaj E.C. Blokland[1,2,3], Prabuddha S. Pathinayake[4], Lan Wei[1], Michael Schuliga[1], Jade Jaffar[5], Glen P. Westall[4], Philip M. Hansbro[1], Cecilia M. Prele[6,7], Steven E. Mutsaers[6,7], Nathan W. Bartlett[1], Janette K. Burgess[3], Christopher L. Grainge[4] and Darryl A. Knight[1,2].

Affiliations:

1. School of Biomedical Sciences and Pharmacy, University of Newcastle, Callaghan, NSW, Australia.
2. National Health and Medical Research Council Centre of Research Excellence in Pulmonary Fibrosis.
3. University of Groningen, University Medical Center Groningen, Dept. of Pathology and Medical Biology, Groningen Research Institute for Asthma and COPD, Groningen, The Netherlands.
4. School of Medicine and Public Health, University of Newcastle, Callaghan, NSW, Australia.
5. Allergy, Immunology and Respiratory Medicine, Alfred Hospital, Prahran, Victoria, Australia.
6. Centre for Cell Therapy and Regenerative Medicine, School of Biomedical Sciences, University of Western Australia, Nedlands, WA, Australia.
7. Institute for Respiratory Health, University of Western Australia, Nedlands, WA, Australia.

Address for Correspondence: Professor Darryl Knight, School of Biomedical Sciences and Pharmacy, University of Newcastle, Callaghan, Australia. (e-mail: darryl.knight@newcastle.edu.au T: +61 02 4921 7485).

Abstract

Idiopathic pulmonary fibrosis (IPF) is a chronic lung disease of unknown cause with a median survival of only 3 years. We and others have shown that fibroblasts derived from IPF-lungs display characteristics of senescent cells and that dysregulated activation of the transcription factor signal transducer and activator of transcription 3 (STAT3) correlates with IPF progression. The question of whether STAT3 activation is involved in fibroblast senescence remains unanswered. We hypothesized that inhibiting STAT3 activation after oxidant-induced senescence would attenuate characteristics of the senescent phenotype. We aimed to characterize a model of oxidant induced senescence in human lung fibroblasts and to determine the effect of inhibiting STAT3 activity on the development of senescence. Exposing human lung fibroblasts to 150µM hydrogen peroxide (H_2O_2) resulted in increased-senescence-associated-β-galactosidase (SA-β-Gal) content, expression of p21 and interleukin (IL)-6, all of which are features of senescence. The shift into senescence was accompanied by an increase of STAT3 translocation to the nucleus and mitochondria. Additionally, Seahorse analysis provided evidence of increased mitochondrial respiration characterized by increased basal respiration, proton leak and an associated increase in superoxide (O_2^-) production in senescent fibroblasts. Targeting STAT3 activity using the small molecule inhibitor STA-21 attenuated IL-6 production, reduced p21 levels, decreased SA-β-Gal accumulation and restored normal mitochondrial function. The results of this study illustrate that stress-induced senescence in lung fibroblasts involves the activation of STAT3 which can be pharmacologically modulated.

AJRCMB Articles in Press. Published on 04-January-2019 as 10.1165/rcmb.2018-0328OC

Key words

Senescence, fibroblast, Signal transducer and activator of transcription 3 (STAT3), mitochondrial dysfunction, cell cycle, fibrosis *

Author Contributions

D.W.W., P.S.P., M.S., C.M.P., S.E.M., N.W.B., J.K.B., C.L.G. and D.A.K. contributed to the concept and design. D.W.W., K.E.C.B., P.S.P., L.W. and J.J. performed the experiments. D.W.W., K.E.C.B., P.S.P., J.J., C.M.P., S.E.M., N.W.B., J.K.B., C.L.G. and D.A.K. analysed and interpreted the data. G.P.W., P.H., C.M.P., S.E.M., N.W.B., J.K.B., C.L.G. and D.A.K. drafted the manuscript and approved the final version for important intellectual content.

* This research was funded by NHMRC grant 1099569 and by the Lung Foundation Australia David Wilson Scholarship awarded to David W. Waters. Janette K. Burgess was supported by a Rosalind Franklin Fellowship co-funded by the University of Groningen and the European Union.

1. Introduction

First recognised by Hayflick and Moorhead in 1961 (1), senescence describes a state of irreversible cell cycle arrest accompanied by an altered secretory profile termed the senescence associated secretory phenotype (SASP). Senescent cells play important roles in wound repair (2), embryogenesis (3), and in preventing pre-malignant cells from dividing (4). The SASP allows senescent cells to signal to other cells within the local environment, promoting differentiation of neighbouring cells, and facilitating self-elimination via immune cells. This self-regulated elimination is a crucial aspect of the phenotype as the persistence of senescent cells is proposed to drive age-related pathologies (5-8). *In vivo*, senescence is a result of excessive rounds of mitotic division, termed replicative senescence (RS), with each event incrementally degrading telomeres culminating in sub-lethal DNA damage.

In vitro, stress induced premature senescence (SIPS) can be induced under various sub-lethal treatment conditions including chemical exposure such as to hydrogen peroxide (H_2O_2) (9), irradiation (10), and UV exposure (11). Cells undergoing SIPS adopt the senescent phenotype earlier in mitotic time than RS-cells but still display hallmark features such as cell cycle arrest and the SASP. Precise origins of SIPS *in vivo* have been difficult to identify but its occurrence is thought to be the decisive factor in the delayed resolution of the age-related pathology of vascular leg ulcers (12). Immune cells, through the release of interferon-γ (IFN-γ) and tumor necrosis factor-α (TNFα), are capable of inflicting sufficient DNA damage to induce senescence in neighbouring cells (13), and mitochondrial dysfunction has also been shown to be capable of driving a cell into premature senescence (14, 15).

AJRCMB Articles in Press. Published on 04-January-2019 as 10.1165/rcmb.2018-0328OC

The chronic lung disease idiopathic pulmonary fibrosis (IPF) is characterised by excessive extracellular matrix (ECM) deposition in the lung likely resulting from an aberrant wound repair response and senescence of the alveolar epithelium (16). While fibroblast senescence is a well-documented feature of explanted cultures from IPF lungs (17, 18), direct evidence for senescent fibroblasts contributing to fibrosis has not emerged. Indeed, evidence from animal models of liver-injury (19), cutaneous wounds (2, 20) and head & neck and oesophageal cancers (21) suggests that senescent fibroblasts may even play an antifibrotic role. This remains to be elucidated in human lung fibrosis.

STAT3 is a latent transcription factor that mediates gene transcription in response to the IL-6 cytokine family (22), IL-10 (23), and a variety of receptor tyrosine kinases (24). Phosphorylation of STAT3 occurs at different residues during separate phosphorylation events, the tyrosine^{705} residue (pSTAT3^{705}) through Janus kinase 1 (JAK1) or JAK2 interaction, or at the serine^{727} residue (pSTAT3^{727}) through the mitogen activated protein kinase/ extracellular-signal-regulated kinase signalling pathway (25). Serine^{727} phosphorylation has been shown to be an additional phosphorylation event to tyrosine^{705} (26, 27), however, it's individual role in gene transcription remains unclear. Once phosphorylated, STAT3 translocates to the nucleus to promote the transcription of target genes, including the anti-apoptotic proteins B-cell lymphoma-extra large and Survivin, cyclin D1 (CCND1), and transcription factors such as c-Myc and Twist-related protein 1 (28). STAT3 also localizes to the mitochondria where it is thought to facilitate optimal functioning of the electron transport chain (ETC) (29, 30).

Constitutively activated STAT3 is a feature of a broad spectrum of cancers (31-33), inflammatory diseases (34), and has been shown to correlate with disease progression in a

cohort of IPF patients (35). Given that STAT3 plays a significant role in transcribing responses to several soluble factors of the SASP, transcription factors such as c-Myc that play a key role in cell cycle progression (36), and also facilitating mitochondrial function, STAT3 potentially represents a novel therapeutic target to modulate features of senescence.

Due to the limited understanding of fibroblast senescence and its impact in the lung we sought to characterize an *in vitro* model of oxidant induced senescence using H_2O_2 and to examine the role and impact of modulating STAT3. We confirmed that senescence is induced in human lung fibroblasts within 72 hrs after exposure to H_2O_2, that STAT3 plays a significant role in cell cycle arrest and increased mitochondrial respiration, and that targeting STAT3 may be a useful approach for modifying senescence.

AJRCMB Articles in Press. Published on 04-January-2019 as 10.1165/rcmb.2018-0328OC

2. Methods

2.1. Cell culture

Primary cultures of lung fibroblasts were established from macroscopically normal lung tissue of patients from the Alfred Hospital, (Melbourne, VC, Australia) and the John Hunter Hospital (Newcastle, NSW, Australia) obtained with informed written consent and approval from the University of Melbourne's Human Research Ethics Committee (HREC980168X), and The Hunter New England Human Research Ethics Committee (HNEHREC 16/07/20/5.03) (Sample demographics in Table S1, detailed methods in online supplement).

2.2. Treatment protocol

Confluent Fibroblast cultures were exposed to 150μM H_2O_2 (Merck) for 2 hrs. After which point, both treated and non-stimulated control fibroblasts had their media removed, were washed twice with a matching volume of PBS (Gibco) and incubated in media containing 0.4% FBS at 37°C in air containing 5% CO_2 for 72 hrs. The influence of STAT3 on the senescent phenotype was assessed using the small molecule inhibitor STA-21 (10μM) (Selleckchem), which was added to cultures 2 hrs after H_2O_2 exposure and maintained throughout the experimental period. All measurements, unless otherwise stated, were obtained 72 hrs after H_2O_2 exposure (detailed methods in online supplement).

2.3. Senescence-associated β-galactosidase staining

Cytochemical staining for SA-β-Gal was performed using a staining kit (Cell Signalling Technology) according to the manufacturer's instructions.

2.4. IL-6 ELISA

Supernatants were centrifuged at 14000 x *g* for 15 minutes to obtain cell-free supernatant used to assay for human interleukin-6 (IL-6) (R&D Systems) according to the manufacturer's instructions.

2.5. Protein quantification and immunoblot

Mitochondrial fractions were isolated using a Mitochondria Isolation Kit (Thermo Scientific). Mitochondrial fractions and fibroblast cultures were lysed with RIPA lysis buffer containing protease (Roche) and phosphatase (Sigma-Aldrich) inhibitors. Protein was subjected to SDS polyacrylamide gel electrophoresis (SDS-PAGE) and transferred to a nitrocellulose membrane (BioRad) in a semi-dry transfer unit (Hoefer™) (Antibodies in Table S2, detailed methods in online supplement).

2.6. mRNA extraction, quantification and PCR

Total messengerRNA (mRNA) was extracted from cultured fibroblast samples using a RNeasy mini kit (Qiagen) according to the manufacturer's instructions (detailed methods in online supplement).

2.7. Immunofluorescence staining

Fibroblasts were fixed with 4% paraformaldehyde and permeabilized with 0.5% Triton X-100/PBS. Cells were incubated with primary antibodies at 4°C overnight followed by incubation with fluorescently labelled secondary antibodies (Cell Signalling Technology) for 1hr at room temperature. Images were visualized using an Axio Imager 2 (Zeiss). Mitochondrial staining

AJRCMB Articles in Press. Published on 04-January-2019 as 10.1165/rcmb.2018-0328OC

was carried out using the MITO-ID detection kit (Enzo Life Sciences) (Antibodies in Table S2) (detailed methods in online supplement).

2.8. Assessment of mitochondrial superoxide production by fluorescence intensity

Mitochondrial generated superoxide was detected using the fluorescent MitoSox probe (Invitrogen) according to the manufacturer's instructions (detailed methods in online supplement).

2.9. Seahorse respiration assay

Mitochondrial function was assessed using the Agilent Seahorse Mito Stress Test Kit (Seahorse Bioscience). Ten thousand cells per well were seeded in a 96-well Seahorse plate, samples were plated in replicates of eight (Protocol setting detailed in online supplement).

2.10. Statistical analysis

Data is presented as individual data points and the mean of all data points of a group. Statistical significance was evaluated using Students paired t-test. Statistical analyses were performed using GraphPad Prism version 7.01. Differences were considered to be statistically significant at $p<0.05$.

3. Results

3.1 Characterization of oxidant induced senescence.

As shown in Figure 1, exposing fibroblasts to 150µM H_2O_2 for 2 hrs induced several features of senescence, including expression of the cyclin-dependent kinase (CDK) inhibitor p21, (Figure 1A, B, C), increased IL-6 secretion indicating a shift in secretory profile (Figure 1D), increased phosphorylated-p53 (pp53) in the nuclei (Figure 1E), and accumulation of cytoplasmic SA-β-Gal (Figure 1F). Taken together, these data suggest that 2 hrs exposure to 150µM H_2O_2 was sufficient to induce senescence in human lung fibroblasts within 72 hrs.

Figure 1. **Fibroblasts shift into a senescent phenotype after H_2O_2 treatment.** Confluent primary human lung fibroblasts with or without 2 hrs exposure to 150µM H_2O_2 were grown for 72 hrs. Supernatants and total cell lysates were collected, A) Immunoblot analyses of fibroblast cultures treated with H_2O_2 and non-stimulated controls (n=6) using specific antibodies against p21, and β-actin as loading control. B) Densitometry values of p21 expression in non-stimulated and H_2O_2 treated cultures (n=6). C) Immunofluorescence staining for p21, in non-stimulated and H_2O_2-treated fibroblasts, blue = DAPI and green = p21. D) IL-6 production measured in the supernatant by ELISA, normalised to mg protein. (n=6). E) Nuclear pp53 content in non-stimulated and H_2O_2-treated lung fibroblasts, blue = DAPI and red = pp53. F) SA-β-Gal content of non-stimulated and H_2O_2-treated fibroblasts, blue = SA-β-Gal. All images are representative (n=3), graphs display the mean with individual data points compared between non-stimulated and H_2O_2 using paired t-test, * $p < 0.05$ (A,C).

AJRCMB Articles in Press. Published on 04-January-2019 as 10.1165/rcmb.2018-0328OC

3.2 Mitochondrial perturbations under oxidant induced senescence.

To further confirm senescence induction we analysed several mitochondrial characteristics as senescent fibroblasts have previously been reported to have higher levels of mitochondrial respiration (37, 38). Accordingly, we tested the mitochondrial function of stress-induced senescent lung fibroblasts. Basal respiration (Figure 2A), proton leak (Figure 2D) and 0_2-generation (Figure 2E) were all significantly increased following exposure to H_20_2. A trend towards an increase in maximal respiration (Figure 2B), and ATP production (Figure 2C) were also observed.

Figure 2. **Increased mitochondrial respiration in fibroblasts after H_2O_2 treatment**. The mitochondrial functions of basal respiration (Figure 2A), maximal respiration (Figure 2B), ATP production (Figure 2C), and proton leak (Figure 2D) were assessed using the Mito Stress Test assay (n=7), OCR is reported per 1000 cells. Mitochondrial superoxide production was measured using a fluorogenic dye specific for the detection of superoxide in the mitochondria (Figure 2E, n=5). All graphs display matched data points compared between non-stimulated and H_2O_2 exposure for each individual patient. Horizontal bars represent group means, * $p < 0.05$ using paired Students t-test.

3.3 Nuclear localization of STAT3 during oxidant-induced senescence

To investigate whether STAT3 localization to the nucleus occurs at a higher rate under oxidant-induced senescence we stained fixed primary lung fibroblast cultures with antibodies

against STAT3, pSTAT3^{705} and DAPI. STAT3 staining can be observed in the nuclei of non-stimulated fibroblasts (Figure 3A), more intense staining can be seen in the nuclei of fibroblasts following exposure to H_20_2 (Figure 3B). pSTAT3^{705} staining can be seen in and around the nuclei of non-stimulated fibroblasts (Figure 3C), pSTAT3^{705} staining is more intense in the nuclei of fibroblasts following H_20_2 exposure (Figure 3D). To confirm increased STAT3 nuclear localization in senescent fibroblasts we analyzed two STAT3 dependent genes using qPCR. Both FN1 (Fibronectin) and CCND1 gene expression levels were increase in H_2O_2 treated cultures compared to non-stimulated cultures (Figure 3E, F).

Figure 3. **Nuclear localisation of STAT3 and pSTAT3^{705} after oxidant induced senescence.** Sub-confluent primary human lung fibroblasts with or without 2 hrs exposure to 150µM H_2O_2 were grown for 72 hrs. Images A and B show nuclear localization of STAT3 in non-stimulated and H_2O_2 treated cultures, images C and D shown nuclear localization of pSTAT3^{705} in non-stimulated and H_2O_2 treated cultures (red = STAT3/ pSTAT3^{705}, blue = DAPI). Each condition has two nuclei highlighted and enlarged for more accurate assessment of localization (i, ii). Images were taken at 63x magnification under oil immersion (n=3). The expression of STAT3 targeted genes FN1 (Figure 3E), and CCND1 (Figure 3F) were analysed by qPCR and normalised against 18 S rRNA. Data is expressed as ΔΔCT (n=6), horizontal bars represent group means, values compared between non-stimulated and H_2O_2-treated using paired t-test, * $p < 0.05$.

AJRCMB Articles in Press. Published on 04-January-2019 as 10.1165/rcmb.2018-0328OC

3.4 *Mitochondrial localization of STAT3 during oxidant-induced senescence*

To identify the presence of activated STAT3 in the mitochondria we isolated mitochondrial fractions from H_2O_2 treated and non-stimulated primary lung fibroblast cultures. A trend towards higher STAT3 and pSTAT3^{705} content in the mitochondrial fractions of H_2O_2 treated cultures can be seen from the immunoblot (Figure 4A). Patient 1 shows an increase in STAT3 and pSTAT3^{705} mitochondrial content after H_2O_2 treatment. Patient 2 shows similar, although not comparable, increases in STAT3 and pSTAT3^{705} (2 bands can be seen in the Patient 2 pSTAT3^{705} blot, the lower band represents pSTAT3^{705}). Patient 3's STAT3 bands show an increase binding in the non-stimulated culture although this is matched by the higher intensity of COX-IV binding. The pSTAT3^{705} bands of Patient 3 show a similar intensity of antibody binding. Additionally, we dual stained fibroblast cultures with a mitochondrial specific dye (MITO-ID) and STAT3/ pSTAT3^{705}. From the separated images in Figure 4B and 4C, STAT3 colocalises with the mitochondrial marker MITO-ID at a similar intensity in non-stimulated cultures (Figure 4B) and those treated with H_2O_2 (Figure 4C). The images in Figure 4D and 4E suggest that under oxidant-induced senescence (Figure 4E) pSTAT3^{705} localizes to the mitochondria at a greater intensity compared to non-stimulated cultures (Figure 4D).

Figure 4. **Mitochondrial localisation of STAT3 and pSTAT3^{705} after oxidant induced senescence.** Sub-confluent primary human lung fibroblasts with or without 2 hrs exposure to 150μM H_2O_2 were grown for 72 hrs. A) immunoblot analyses of fibroblast cultures treated with H_2O_2 and non-stimulated controls (n=3) using specific antibodies against STAT3, pSTAT3^{705} and COX-IV as a mitochondria specific loading control. Images B - E illustrate mitochondrial localization of STAT3 and pSTAT3^{705} in non-stimulated and H_2O_2 treated

fibroblasts by immunofluorescence (green = mitochondria, red = STAT3/ pSTAT3^{705}, blue = DAPI). All images have a yellow box representing an area that has been magnified, split into mitochondria only, STAT3/ pSTAT3^{705} only, and an enlarged merged image.

3.5 STA-21 inhibits nuclear and mitochondrial STAT3 content.

To confirm inhibition of STAT3 activity after STA-21 treatment, sub-confluent primary human lung fibroblasts treated with 150μM H_2O_2 with or without the addition of 10μM STA-21 were grown for 72 hrs. We proceeded to fix and stain fibroblast cultures with antibodies against STAT3, pSTAT3^{705}, DAPI, and the mitochondrial specific dye MITO-ID. The presence of nuclear STAT3 is more abundant in the H_2O_2 only treatment group (Figure 5A), the addition of STA-21 reduces nuclear content of STAT3 (Figure 5B). Images 5D shows a marked reduction in nuclear pSTAT3^{705} in those fibroblasts treated with STA-21 compared to the H_2O_2 condition alone (Figure 5C). The reduced cellular-content of STAT3 after the addition of STA-21 results in a decrease in the intensity of overlap between STAT3 and the mitochondria (Figure 5F) compared to H_2O_2 only treatment group (Figure 5E). The subsequent reduction of pSTAT3^{705} after the addition of STA-21 similarly reflects reduced mitochondrial overlap with the addition of STA-21 (Figure 5H) compared to H_2O_2 only (Figure 5G).

AJRCMB Articles in Press. Published on 04-January-2019 as 10.1165/rcmb.2018-0328OC

Figure 5. nuclear and mitochondrial localization of STAT3 and pSTAT3^{705} after STAT3 inhibition. Sub-confluent primary human lung fibroblasts treated with 150μM H_2O_2 with or without the addition of 10μM STA-21 were grown for 72 hrs. Images A - D show the nuclear localization of STAT3 and pSTAT3^{705} (red = STAT3/ pSTAT3^{705}, blue = DAPI). Each condition has two nuclei highlighted and enlarged for more accurate assessment of localization (i, ii). Images E-H describe mitochondrial localization of STAT3 and pSTAT3^{705} (green = mitochondria, red = STAT3/ pSTAT3705, blue = DAPI). Each condition has 3 separate images enlarged to highlight mitochondria only, STAT3/ pSTAT3^{705} only, and a merged image. Images were taken at 63x magnification under oil immersion (n=3).

3.6 *The effect of inhibiting STAT3 activity on oxidant induced senescence.*

Given that STAT3 nuclear and mitochondrial translocation increases during oxidant-induced senescence, we next examined the effect of inhibiting STAT3 on senescence induction. We found that treatment with STA-21 supressed levels of p21, as measured by immunoblot (Figure 6A) confirmed by graphed densitometry (Figure 6B), and reduced staining of p21 in the nuclei of H_2O_2-treated fibroblasts (Figure 6C). Reduced IL-6 secretion suggests an attenuated secretory profile (Figure 6D), and decreased SA-β-Gal content measured using a cytochemical assay (Figure 6E). Taken together our data suggests that inhibition of STAT3 can attenuate the shift into senescence of human lung fibroblasts.

Figure 6. **STAT3 inhibition attenuates the shift into senescence**. Confluent primary human lung fibroblasts treated with 150μM H_2O_2 with or without the addition of 10μM STA-21 were

grown for 72 hrs. STAT3 inhibition resulted in a reduction of p21, (A) immunoblot analyses of fibroblast cultures treated with H_2O_2 only and H_2O_2 + STA-21 (STA-21) (n=5) using specific antibodies against p21, and β-actin as loading control. B) graphed densitometry of a p21 immunoblot after H_2O_2 only and with the addition of STA-21, (n=4), densitometric analysis of Patient 2 from Figure 6A was not possible due to insufficient resolution of p21 band. C) Immunofluorescence of fibroblasts stained for p21 (blue = DAPI and green = p21). IL-6 production measured in the supernatant by ELISA (D), normalised to mg protein. (n=6). E) SA-β-Gal content (blue = SA-β-Gal). Graphs displays the mean, individual data points were compared between H_2O_2 and the addition of STA-21 (H_2O_2 + STA-21) using paired Students t-test (A, B). All images are representative (n=3).

3.7 Inhibiting STAT3 activity lowers mitochondrial respiration after oxidant induced senescence.

To further assess the effect of inhibiting STAT3 activation on senescence we investigated its effect on mitochondrial function. Figure 7 shows that the inhibition of STAT3 activity prevents senescence-induced increases in mitochondrial respiration. Oxygen consumption rate values for basal respiration (Figure 7A), maximal respiration (Figure 7B), ATP production (Figure 7C), and proton leak (Figure 7D) were all reduced to values comparable to non-stimulated cultures after STAT3 inhibition in all but one patient sample. Superoxide generation was also substantially attenuated after STAT3 inhibition (Figure 7E). Together, these data suggest that the inhibition of STAT3 restores normal mitochondrial function.

AJRCMB Articles in Press. Published on 04-January-2019 as 10.1165/rcmb.2018-0328OC

Figure 7. Mitochondrial function is restored after STAT3 inhibition. The mitochondrial functions of basal respiration (Figure 7A), maximal respiration (Figure 7B), ATP production (Figure 7C), and proton leak (Figure 7D) were again assessed using the Mito Stress Test assay (n=7), OCR is reported per 1000 cells. Mitochondrial superoxide production measured using the same fluorogenic dye specific for mitochondrial superoxide as previous (Figure 7E, n=5). All graphs display matched data points compared between fibroblasts treated with H_2O_2 only and fibroblasts treated with H_2O_2 and STA-21 2-hrs after H_2O_2 treatment (H_2O_2 + STA-21) using paired Students t-test (A-E).

5. Discussion

Senescence is associated with ageing, as is the fibrotic lung disease IPF. The influence of senescent cells in the pathogenesis of lung fibrosis is uncertain. On one hand, Lehmann et al. showed that senescent alveolar epithelial cells are profibrotic (16), whereas the available data on senescent fibroblasts suggests they maybe anti-fibrotic (39, 40). In this study we characterized a model of oxidant-induced senescence and identified the transcription factor STAT3 as playing a key role in the fibroblasts shift into senescence. Furthermore, the onset of senescence could be attenuated by inhibiting STAT3 activation.

The use of H_2O_2 has previously been described to induce senescence in the IMR-90 human fibroblast cell line (41). Here we have extended previous work to primary human lung fibroblasts and characterized in detail senescence following H_2O_2 treatment. We observed increased p21 expression, IL-6 production, cytoplasmic SA-β-Gal and pp53 following H_20_2 exposure, which are all recognized characteristics of senescent cells (42). Increased mitochondrial respiration was also a feature of H_2O_2 treated fibroblasts, a characteristic previously described as being a feature of fibroblasts undergoing replicative senescence (37, 38).

Under normal conditions the phosphorylation of p53 is tightly regulated but in response to stress p53 becomes activated and translocates to the nucleus to target genes involved in DNA repair and cell-cycle arrest (43). The increased pp53 observed in the fibroblasts of this study is a result of the DNA-damage-response after H_2O_2 exposure. The increased pp53 promotes the transcription of p21 culminating in cell cycle arrest of H_2O_2 treated cultures. Mitotic arrest has

AJRCMB Articles in Press. Published on 04-January-2019 as 10.1165/rcmb.2018-0328OC

been shown to be mediated by the p21/p53 axis in both the G1 and G2 phases of the cell cycle (44, 45). The increased p53 activity also has the potential to influence the secretory profile of senescent fibroblasts as p53 is capable of binding to the IL-6 promoter to drive transcription (46).

Association between STAT3 and the onset of senescence are well documented (reviewed in (47)) and STAT3 activity is strongly associated with interstitial lung diseases such as IPF (35, 48-50). In this study, we identified STAT3 as playing a key role in the shift of secretory profile, cell cycle arrest, and mitochondrial respiration. Our results suggest STAT3 is an important factor driving the onset of the senescent phenotype, and supports previous work showing that JAK1/2 inhibition alleviates the onset of senescence (51, 52).

Given the impact that inhibiting STAT3 activity had on senescence, it was surprising that the kinetics of phosphorylation did not differ between non-stimulated and those fibroblasts driven into senescence (Supplementary Figure 1). Increases in STAT3 and pSTAT3^{705} levels in senescent cultures were observed across a 72-hour time course but not consistently. However, the nuclear localization of both non-phosphorylated STAT3 (npSTAT3) and pSTAT3^{705} in senescent cells was significantly greater than in non-senescent cells. Additionally, we observed increased expression of the FN1 and CCND1 genes, both known targets of STAT3 (53, 54). Interestingly, RS-fibroblasts have been shown to express five-fold higher levels of the associated CCND1 protein than low-passage fibroblasts (55).

We speculate that the increased nuclear pSTAT3^{705} promotes the transcription of target genes driving the shift into senescence. The role of npSTAT3 in and around the nucleus of senescent

fibroblasts is unclear. Studies have shown that npSTAT3 plays an important role in transcription; being responsible for promoting the transcription of a discreet set of genes not transcriptionally activated by pSTAT3^{705} (56). How transcriptional activation occurs through npSTAT3 is yet to be confirmed but binding to other transcription factors is plausible since a similar mechanism has been described for the structurally similar STAT1 (57, 58). In addition, we also sought to identify whether STAT3 or pSTAT3^{705} localized to the mitochondria at a greater intensity in those fibroblasts induced into senescence. Both STAT3 and pSTAT3^{705} have previously been identified in the mitochondria where they influence the ETC (29, 30). We observed increases in both STAT3 and pSTAT3^{705} in isolated mitochondrial fractions from senescent fibroblasts. The increased mitochondrial presence of STAT3 and pSTAT3^{705} in senescent fibroblasts may be exerting a negative influence on ETC dynamics resulting in increased respiration and proton leak.

pSTAT3^{705} has been shown to promote the transcription of the STAT3 gene (59) and so the addition of STA-21 to the H_2O_2 treated fibroblasts not only reduced nuclear localization but also resulted in a reduction in cellular content of STAT3. We speculate that the reduced STAT3, and pSTAT3^{705} of senescent fibroblasts had a proportional effect on reducing mitochondrial interactions potentially enabling the ECT to function in a manner similar to non-H_2O_2-stimulated conditions. The fibroblasts from one patient did not conform with the response of others which precluded group statistical significance.

The mean age of patient samples used in this study was 58 years. Seven of the samples were from patients over the age of 65, the age typically associated with a diagnosis of IPF. We do not think that the age of the patients influenced the results of this study. We acknowledge that

AJRCMB Articles in Press. Published on 04-January-2019 as 10.1165/rcmb.2018-0328OC

older patients may have a higher incidence of RS-cells however a large proportion of fibroblasts from these patients would still be susceptible to oxidant-induced senescence. Our use of oxidative stress to induce senescence is an important consideration in regard to senescence-associated respiratory disease. The lungs are continuously exposed to endogenous and exogenous oxidants with diffuse lung diseases such as IPF are associated with a pulmonary redox imbalance (60).

The use of STA-21 to alleviate senescence suggests that there is potential for the use of small molecule inhibitors as therapeutics to rescue the phenotype of senescent cells. STA-21 is sufficient to block dimerization of pSTAT3^{705} monomers but it does not cover the amino acid reside Ser^{727}, thus it is ineffective at preventing the formation of pSTAT3^{727} dimers. Future studies should investigate STAT3 inhibitors that also cover the Ser^{727} residue should it be shown that pSTAT3^{727} is also capable of promoting transcription independent of phosphorylation at Tyr^{705}.

Pharmacological intervention using senolytics is currently being investigated for the targeted removal of senescent cells (61). However, this approach should be explored with caution as these drugs indiscriminately target senescent cells for removal regardless of cell-type. If therapeutic targeting of senescent cells becomes recognized as a viable treatment option for fibrotic diseases, an approach that restores the normal phenotype of a targeted-cell and maintains its presence *in situ* is preferable to one that destroys a problem-cell outright, potentially decellularising a region of tissue *en mass*.

In conclusion, we have shown that senescence can be modelled in primary cultures of human lung fibroblasts and that the inhibition of STAT3-activation and its subsequent reduction in the nuclei and mitochondria is a decisive factor in attenuating senescence induction. Future studies should utilize the model to identify the contribution of senescent fibroblasts to fibrotic diseases such as IPF and to determine whether STAT3 activity is also a feature of epithelial cell senescence. The relative ease of targeting epithelial cells may facilitate the use of STAT3 inhibitors as potential therapeutics to abate their proposed profibrotic phenotype.

AJRCMB Articles in Press. Published on 04-January-2019 as 10.1165/rcmb.2018-0328OC

References

1. Hayflick L, Moorhead PS. The serial cultivation of human diploid cell strains. Experimental cell research. 1961;25:585-621.
2. Demaria M, Ohtani N, Youssef Sameh A, Rodier F, Toussaint W, Mitchell James R, et al. An Essential Role for Senescent Cells in Optimal Wound Healing through Secretion of PDGF-AA. Developmental Cell.31(6):722-33.
3. Muñoz-Espín D, Cañamero M, Maraver A, Gómez-López G, Contreras J, Murillo-Cuesta S, et al. Programmed Cell Senescence during Mammalian Embryonic Development. Cell.155(5):1104-18.
4. Dimri GP. What has senescence got to do with cancer? Cancer cell. 2005;7(6):505-12.
5. van Deursen JM. The role of senescent cells in ageing. Nature. 2014;509(7501):439-46.
6. Tchkonia T, Zhu Y, van Deursen J, Campisi J, Kirkland JL. Cellular senescence and the senescent secretory phenotype: therapeutic opportunities. The Journal of clinical investigation. 2013;123(3):966-72.
7. Xue W, Zender L, Miething C, Dickins RA, Hernando E, Krizhanovsky V, et al. Senescence and tumour clearance is triggered by p53 restoration in murine liver carcinomas. Nature. 2007;445(7128):656-60.
8. Kang TW, Yevsa T, Woller N, Hoenicke L, Wuestefeld T, Dauch D, et al. Senescence surveillance of pre-malignant hepatocytes limits liver cancer development. Nature. 2011;479(7374):547-51.
9. Chen JH, Ozanne SE, Hales CN. Methods of cellular senescence induction using oxidative stress. Methods in molecular biology (Clifton, NJ). 2007;371:179-89.
10. Wang Y, Boerma M, Zhou D. Ionizing Radiation-Induced Endothelial Cell Senescence and Cardiovascular Diseases. Radiation research. 2016;186(2):153-61.
11. Debacq-Chainiaux F, Leduc C, Verbeke A, Toussaint O. UV, stress and aging. Dermato-endocrinology. 2012;4(3):236-40.
12. Harding KG, Moore K, Phillips TJ. Wound chronicity and fibroblast senescence – implications for treatment. International Wound Journal. 2005;2(4):364-8.
13. Braumuller H, Wieder T, Brenner E, Assmann S, Hahn M, Alkhaled M, et al. T-helper-1-cell cytokines drive cancer into senescence. Nature. 2013;494(7437):361-5.
14. Wiley Christopher D, Velarde Michael C, Lecot P, Liu S, Sarnoski Ethan A, Freund A, et al. Mitochondrial Dysfunction Induces Senescence with a Distinct Secretory Phenotype. Cell Metabolism. 2016;23(2):303-14.
15. Schuliga M, Pechkovsky DV, Read J, Waters DW, Blokland KEC, Reid AT, et al. Mitochondrial dysfunction contributes to the senescent phenotype of IPF lung fibroblasts. Journal of Cellular and Molecular Medicine.0(0).
16. Lehmann M, Korfei M, Mutze K, Klee S, Skronska-Wasek W, Alsafadi HN, et al. Senolytic drugs target alveolar epithelial cell function and attenuate experimental lung fibrosis ex vivo. European Respiratory Journal. 2017;50(2).

17. Schafer MJ, White TA, Iijima K, Haak AJ, Ligresti G, Atkinson EJ, et al. Cellular senescence mediates fibrotic pulmonary disease. Nature Communications. 2017;8:14532.
18. Alvarez D, Cardenes N, Sellares J, Bueno M, Corey C, Hanumanthu VS, et al. IPF lung fibroblasts have a senescent phenotype. American journal of physiology Lung cellular and molecular physiology. 2017;313(6):L1164-l73.
19. Krizhanovsky V, Yon M, Dickins RA, Hearn S, Simon J, Miething C, et al. Senescence of activated stellate cells limits liver fibrosis. Cell. 2008;134(4):657-67.
20. Jun JI, Lau LF. The matricellular protein CCN1 induces fibroblast senescence and restricts fibrosis in cutaneous wound healing. Nature cell biology. 2010;12(7):676-85.
21. Mellone M, Hanley CJ, Thirdborough S, Mellows T, Garcia E, Woo J, et al. Induction of fibroblast senescence generates a non-fibrogenic myofibroblast phenotype that differentially impacts on cancer prognosis. Aging (Albany NY). 2016;9(1):114-32.
22. Aggarwal BB, Kunnumakkara AB, Harikumar KB, Gupta SR, Tharakan ST, Koca C, et al. Signal transducer and activator of transcription-3, inflammation, and cancer: how intimate is the relationship? Annals of the New York Academy of Sciences. 2009;1171:59-76.
23. Hutchins AP, Diez D, Miranda-Saavedra D. The IL-10/STAT3-mediated anti-inflammatory response: recent developments and future challenges. Briefings in Functional Genomics. 2013;12(6):489-98.
24. Song L, Turkson J, Karras JG, Jove R, Haura EB. Activation of Stat3 by receptor tyrosine kinases and cytokines regulates survival in human non-small cell carcinoma cells. Oncogene. 2003;22(27):4150-65.
25. Chung J, Uchida E, Grammer TC, Blenis J. STAT3 serine phosphorylation by ERK-dependent and -independent pathways negatively modulates its tyrosine phosphorylation. Mol Cell Biol. 1997;17(11):6508-16.
26. Bhattacharya S, Ray Ramesh M, Johnson Leonard R. STAT3-mediated transcription of Bcl-2, Mcl-1 and c-IAP2 prevents apoptosis in polyamine-depleted cells. Biochemical Journal. 2005;392(Pt 2):335-44.
27. Mufson RA. The role of serine/threonine phosphorylation in hematopoietic cytokine receptor signal transduction. Faseb j. 1997;11(1):37-44.
28. Macias E, Rao D, DiGiovanni J. Role of Stat3 in Skin Carcinogenesis: Insights Gained from Relevant Mouse Models. Journal of Skin Cancer. 2013;2013:10.
29. Gough DJ, Corlett A, Schlessinger K, Wegrzyn J, Larner AC, Levy DE. Mitochondrial STAT3 supports Ras-dependent oncogenic transformation. Science (New York, NY). 2009;324(5935):1713-6.
30. Wegrzyn J, Potla R, Chwae YJ, Sepuri NB, Zhang Q, Koeck T, et al. Function of mitochondrial Stat3 in cellular respiration. Science (New York, NY). 2009;323(5915):793-7.
31. Darnell JE. Validating Stat3 in cancer therapy. Nature medicine. 2005;11(6):595-6.
32. Yu H, Pardoll D, Jove R. STATs in cancer inflammation and immunity: a leading role for STAT3. Nature reviews Cancer. 2009;9(11):798-809.
33. Yue P, Turkson J. Targeting STAT3 in cancer: how successful are we? Expert opinion on investigational drugs. 2009;18(1):45-56.

AJRCMB Articles in Press. Published on 04-January-2019 as 10.1165/rcmb.2018-0328OC

34. Grivennikov S, Karin E, Terzic J, Mucida D, Yu GY, Vallabhapurapu S, et al. IL-6 and Stat3 are required for survival of intestinal epithelial cells and development of colitis-associated cancer. Cancer cell. 2009;15(2):103-13.
35. Pechkovsky DV, Prele CM, Wong J, Hogaboam CM, McAnulty RJ, Laurent GJ, et al. STAT3-mediated signaling dysregulates lung fibroblast-myofibroblast activation and differentiation in UIP/IPF. Am J Pathol. 2012;180(4):1398-412.
36. Hanson KD, Shichiri M, Follansbee MR, Sedivy JM. Effects of c-myc expression on cell cycle progression. Molecular and Cellular Biology. 1994;14(9):5748-55.
37. Kim SJ, Mehta HH, Wan J, Kuehnemann C, Chen J, Hu JF, et al. Mitochondrial peptides modulate mitochondrial function during cellular senescence. Aging (Albany NY). 2018.
38. Hutter E, Renner K, Pfister G, Stöckl P, Jansen-Dürr P, Gnaiger E. Senescence-associated changes in respiration and oxidative phosphorylation in primary human fibroblasts. Biochemical Journal. 2004;380(Pt 3):919-28.
39. Cui H, Ge J, Xie N, Banerjee S, Zhou Y, Antony VB, et al. miR-34a Inhibits Lung Fibrosis by Inducing Lung Fibroblast Senescence. American Journal of Respiratory Cell and Molecular Biology. 2017;56(2):168-78.
40. Li Y, Liang J, Yang T, Mena JM, Huan C, Xie T, et al. Hyaluronan synthase 2 regulates fibroblast senescence in pulmonary fibrosis. Matrix biology : journal of the International Society for Matrix Biology. 2016;55:35-48.
41. Zdanov S, Remacle J, Toussaint O. Establishment of H2O2-induced premature senescence in human fibroblasts concomitant with increased cellular production of H2O2. Annals of the New York Academy of Sciences. 2006;1067:210-6.
42. Campisi J. Aging, cellular senescence, and cancer. Annual review of physiology. 2013;75:685-705.
43. Kachnic LA, Wu B, Wunsch H, Mekeel KL, DeFrank JS, Tang W, et al. The Ability of p53 to Activate Downstream Genes p21 WAF1/cip1 and MDM2, and Cell Cycle Arrest following DNA Damage Is Delayed and Attenuated in scid Cells Deficient in the DNA-dependent Protein Kinase. Journal of Biological Chemistry. 1999;274(19):13111-7.
44. Baus F, Gire V, Fisher D, Piette J, Dulic V. Permanent cell cycle exit in G2 phase after DNA damage in normal human fibroblasts. Embo j. 2003;22(15):3992-4002.
45. Chang B-D, Broude EV, Fang J, Kalinichenko TV, Abdryashitov R, Poole JC, et al. p21Waf1/Cip1/Sdi1-induced growth arrest is associated with depletion of mitosis-control proteins and leads to abnormal mitosis and endoreduplication in recovering cells. Oncogene. 2000;19:2165.
46. Lowe JM, Menendez D, Bushel PR, Shatz M, Kirk EL, Troester MA, et al. p53 and NF-kappaB coregulate proinflammatory gene responses in human macrophages. Cancer research. 2014;74(8):2182-92.
47. Waters DW, Blokland KEC, Pathinayake PS, Burgess JK, Mutsaers SE, Prele CM, et al. Fibroblast senescence in the pathology of idiopathic pulmonary fibrosis. American journal of physiology Lung cellular and molecular physiology. 2018.
48. Fabre A, Marchal S, Forbes LR, Vogel TP, Barlogis V, Triolo V, et al. STAT3 GOF: A New Kid on the Block in Interstitial Lung Diseases. American Journal of Respiratory and Critical Care Medicine.0(ja):null.

49. Flanagan SE, Haapaniemi E, Russell MA, Caswell R, Allen HL, De Franco E, et al. Activating germline mutations in STAT3 cause early-onset multi-organ autoimmune disease. Nature genetics. 2014;46(8):812-4.
50. Haapaniemi EM, Kaustio M, Rajala HLM, van Adrichem AJ, Kainulainen L, Glumoff V, et al. Autoimmunity, hypogammaglobulinemia, lymphoproliferation, and mycobacterial disease in patients with activating mutations in STAT3. Blood. 2015;125(4):639-48.
51. Xu M, Tchkonia T, Ding H, Ogrodnik M, Lubbers ER, Pirtskhalava T, et al. JAK inhibition alleviates the cellular senescence-associated secretory phenotype and frailty in old age. Proc Natl Acad Sci U S A. 2015;112(46):E6301-10.
52. Toso A, Revandkar A, Di Mitri D, Guccini I, Proietti M, Sarti M, et al. Enhancing chemotherapy efficacy in Pten-deficient prostate tumors by activating the senescence-associated antitumor immunity. Cell reports. 2014;9(1):75-89.
53. Luo J, Yan R, He X, He J. Constitutive activation of STAT3 and cyclin D1 overexpression contribute to proliferation, migration and invasion in gastric cancer cells. American journal of translational research. 2017;9(12):5671-7.
54. Pechkovsky DV, Prêle CM, Wong J, Hogaboam CM, McAnulty RJ, Laurent GJ, et al. STAT3-Mediated Signaling Dysregulates Lung Fibroblast-Myofibroblast Activation and Differentiation in UIP/IPF. The American Journal of Pathology. 2012;180(4):1398-412.
55. Atadja P, Wong H, Veillette C, Riabowol K. Overexpression of cyclin D1 blocks proliferation of normal diploid fibroblasts. Experimental cell research. 1995;217(2):205-16.
56. Yang J, Chatterjee-Kishore M, Staugaitis SM, Nguyen H, Schlessinger K, Levy DE, et al. Novel roles of unphosphorylated STAT3 in oncogenesis and transcriptional regulation. Cancer research. 2005;65(3):939-47.
57. Horvath CM, Stark GR, Kerr IM, Darnell JE, Jr. Interactions between STAT and non-STAT proteins in the interferon-stimulated gene factor 3 transcription complex. Mol Cell Biol. 1996;16(12):6957-64.
58. Souissi I, Ladam P, Cognet JAH, Le Coquil S, Varin-Blank N, Baran-Marszak F, et al. A STAT3-inhibitory hairpin decoy oligodeoxynucleotide discriminates between STAT1 and STAT3 and induces death in a human colon carcinoma cell line. Molecular Cancer. 2012;11:12-.
59. Ichiba M, Nakajima K, Yamanaka Y, Kiuchi N, Hirano T. Autoregulation of the Stat3 Gene through Cooperation with a cAMP-responsive Element-binding Protein. Journal of Biological Chemistry. 1998;273(11):6132-8.
60. Kinnula VL, Vuorinen K, Ilumets H, Rytila P, Myllarniemi M. Thiol proteins, redox modulation and parenchymal lung disease. Current medicinal chemistry. 2007;14(2):213-22.
61. Zhu Y, Doornebal EJ, Pirtskhalava T, Giorgadze N, Wentworth M, Fuhrmann-Stroissnigg H, et al. New agents that target senescent cells: the flavone, fisetin, and the BCL-X_L inhibitors, A1331852 and A1155463. Aging. 2017;9(3):955-63.

AJRCMB Articles in Press. Published on 04-January-2019 as 10.1165/rcmb.2018-0328OC

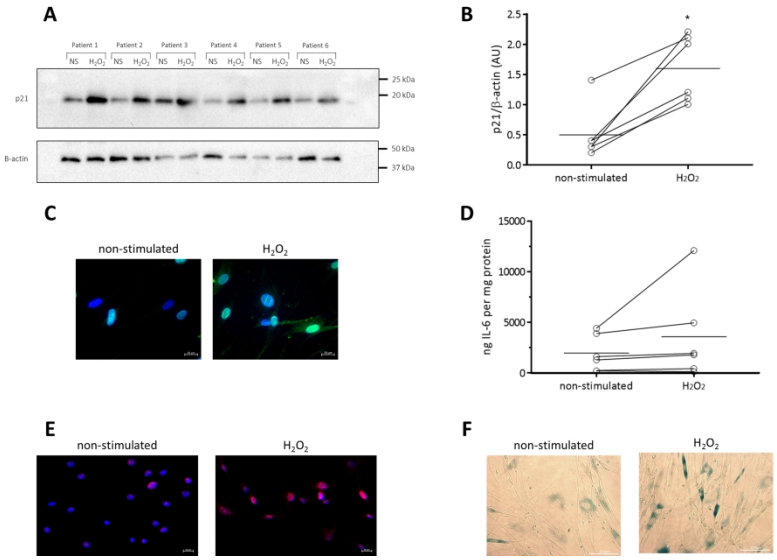

Figure 1. Fibroblasts shift into a senescent phenotype after H2O2 treatment. Confluent primary human lung fibroblasts with or without 2 hrs exposure to 150μM H2O2 were grown for 72 hrs. Supernatants and total cell lysates were collected, A) Immunoblot analyses of fibroblast cultures treated with H2O2 and non-stimulated controls (n=6) using specific antibodies against p21, and β-actin as loading control. B) Densitometry values of p21 expression in non-stimulated and H2O2 treated cultures (n=6). C) Immunofluorescence staining for p21, in non-stimulated and H2O2-treated fibroblasts, blue = DAPI and green = p21. D) IL-6 production measured in the supernatant by ELISA, normalised to mg protein. (n=6). E) Nuclear pp53 content in non-stimulated and H2O2-treated lung fibroblasts, blue = DAPI and red = pp53. F) SA-β-Gal content of non-stimulated and H2O2-treated fibroblasts, blue = SA-β-Gal. All images are representative (n=3), graphs display the mean with individual data points compared between non-stimulated and H2O2 using paired t-test, * p <0.05 (A,C).

338x190mm (300 x 300 DPI)

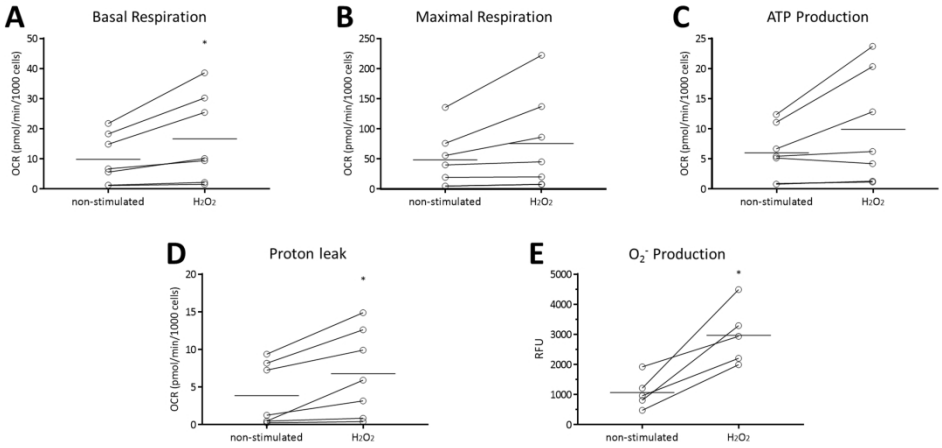

Figure 2. Increased mitochondrial respiration in fibroblasts after H2O2 treatment. The mitochondrial functions of basal respiration (Figure 2A), maximal respiration (Figure 2B), ATP production (Figure 2C), and proton leak (Figure 2D) were assessed using the Mito Stress Test assay (n=7), OCR is reported per 1000 cells. Mitochondrial superoxide production was measured using a fluorogenic dye specific for the detection of superoxide in the mitochondria (Figure 2E, n=5). All graphs display matched data points compared between non-stimulated and H2O2 exposure for each individual patient. Horizontal bars represent group means, * p <0.05 using paired Students t-test.

338x190mm (300 x 300 DPI)

AJRCMB Articles in Press. Published on 04-January-2019 as 10.1165/rcmb.2018-0328OC

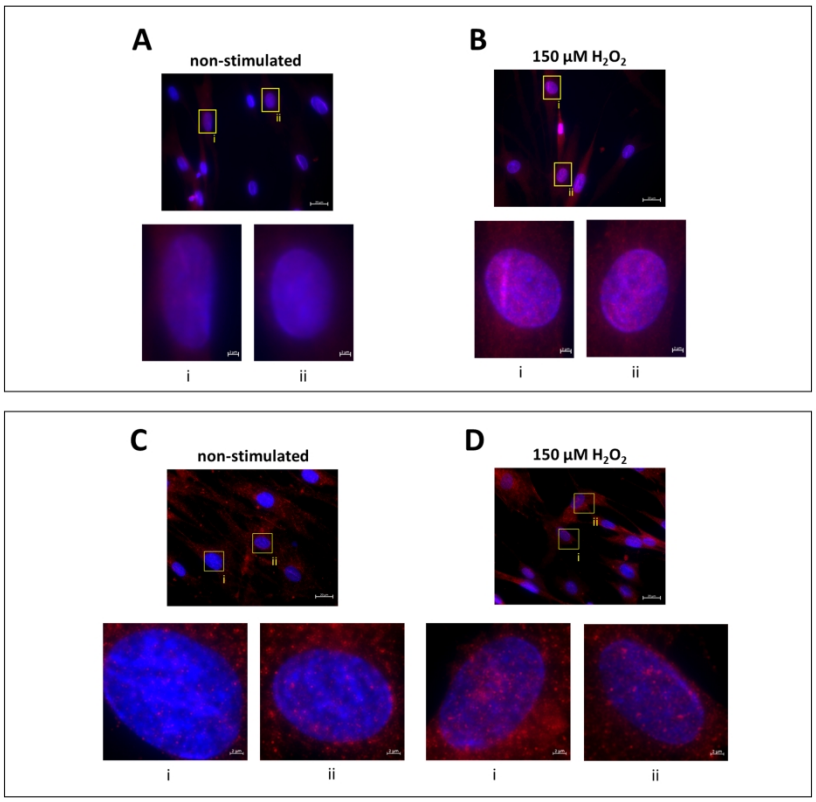

Figure 3. Nuclear localisation of STAT3 and pSTAT3705 after oxidant induced senescence. Sub-confluent primary human lung fibroblasts with or without 2 hrs exposure to 150µM H2O2 were grown for 72 hrs. Images A and B show nuclear localization of STAT3 in non-stimulated and H2O2 treated cultures, images C and D shown nuclear localization of pSTAT3705 in non-stimulated and H2O2 treated cultures (red = STAT3/ pSTAT3705, blue = DAPI). Each condition has two nuclei highlighted and enlarged for more accurate assessment of localization (i, ii). Images were taken at 63x magnification under oil immersion (n=3). The expression of STAT3 targeted genes FN1 (Figure 3E), and CCND1 (Figure 3F) were analysed by qPCR and normalised against 18 S rRNA. Data is expressed as ΔΔCT (n=6), horizontal bars represent group means, values compared between non-stimulated and H2O2-treated using paired t-test, * p <0.05.

338x399mm (300 x 300 DPI)

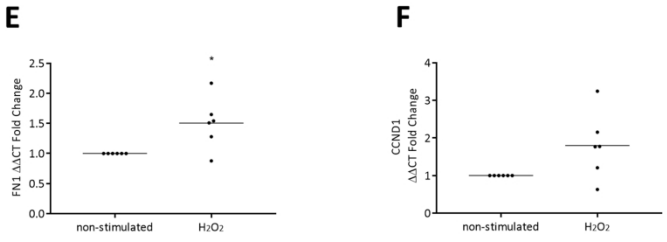

Figure 3. Nuclear localisation of STAT3 and pSTAT3705 after oxidant induced senescence. Sub-confluent primary human lung fibroblasts with or without 2 hrs exposure to 150μM H2O2 were grown for 72 hrs. Images A and B show nuclear localization of STAT3 in non-stimulated and H2O2 treated cultures, images C and D shown nuclear localization of pSTAT3705 in non-stimulated and H2O2 treated cultures (red = STAT3/ pSTAT3705, blue = DAPI). Each condition has two nuclei highlighted and enlarged for more accurate assessment of localization (i, ii). Images were taken at 63x magnification under oil immersion (n=3). The expression of STAT3 targeted genes FN1 (Figure 3E), and CCND1 (Figure 3F) were analysed by qPCR and normalised against 18 S rRNA. Data is expressed as ΔΔCT (n=6), horizontal bars represent group means, values compared between non-stimulated and H2O2-treated using paired t-test, * p <0.05.

338x399mm (300 x 300 DPI)

AJRCMB Articles in Press. Published on 04-January-2019 as 10.1165/rcmb.2018-0328OC

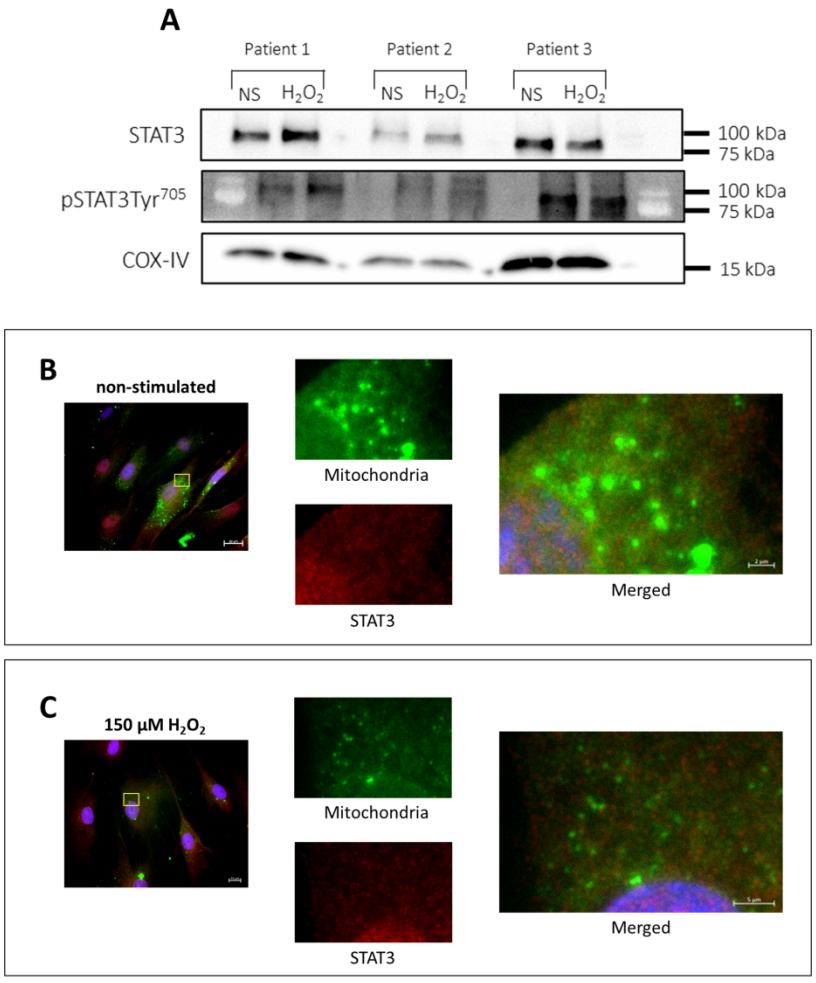

Figure 4. Mitochondrial localisation of STAT3 and pSTAT3705 after oxidant induced senescence. Sub-confluent primary human lung fibroblasts with or without 2 hrs exposure to 150µM H2O2 were grown for 72 hrs. A) immunoblot analyses of fibroblast cultures treated with H2O2 and non-stimulated controls (n=3) using specific antibodies against STAT3, pSTAT3705 and COX-IV as a mitochondria specific loading control. Images B - E illustrate mitochondrial localization of STAT3 and pSTAT3705 in non-stimulated and H2O2 treated fibroblasts by immunofluorescence (green = mitochondria, red = STAT3/ pSTAT3705, blue = DAPI). All images have a yellow box representing an area that has been magnified, split into mitochondria only, STAT3/ pSTAT3705 only, and an enlarged merged image.

338x400mm (300 x 300 DPI)

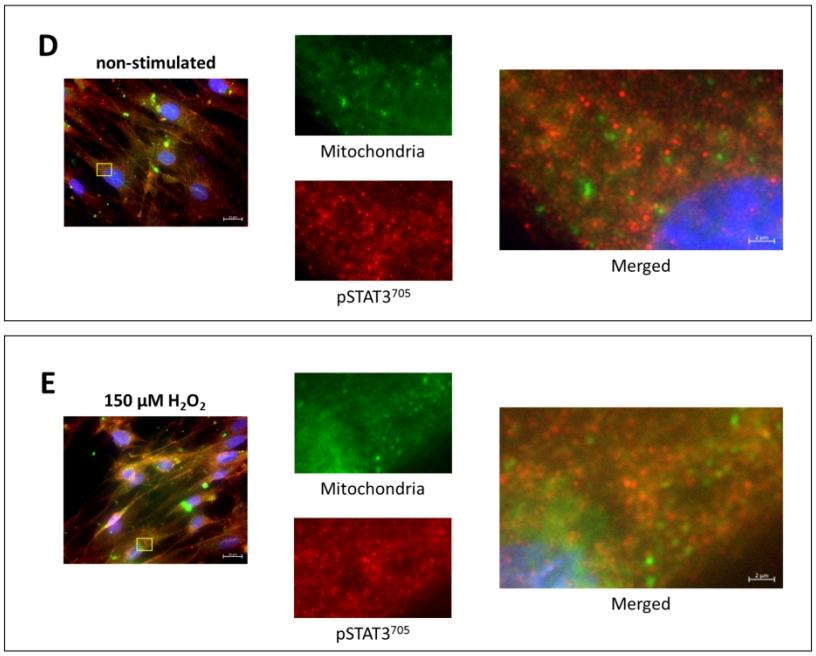

Figure 4. Mitochondrial localisation of STAT3 and pSTAT3705 after oxidant induced senescence. Sub-confluent primary human lung fibroblasts with or without 2 hrs exposure to 150µM H2O2 were grown for 72 hrs. A) immunoblot analyses of fibroblast cultures treated with H2O2 and non-stimulated controls (n=3) using specific antibodies against STAT3, pSTAT3705 and COX-IV as a mitochondria specific loading control. Images B - E illustrate mitochondrial localization of STAT3 and pSTAT3705 in non-stimulated and H2O2 treated fibroblasts by immunofluorescence (green = mitochondria, red = STAT3/ pSTAT3705, blue = DAPI). All images have a yellow box representing an area that has been magnified, split into mitochondria only, STAT3/ pSTAT3705 only, and an enlarged merged image.

338x400mm (300 x 300 DPI)

AJRCMB Articles in Press. Published on 04-January-2019 as 10.1165/rcmb.2018-0328OC

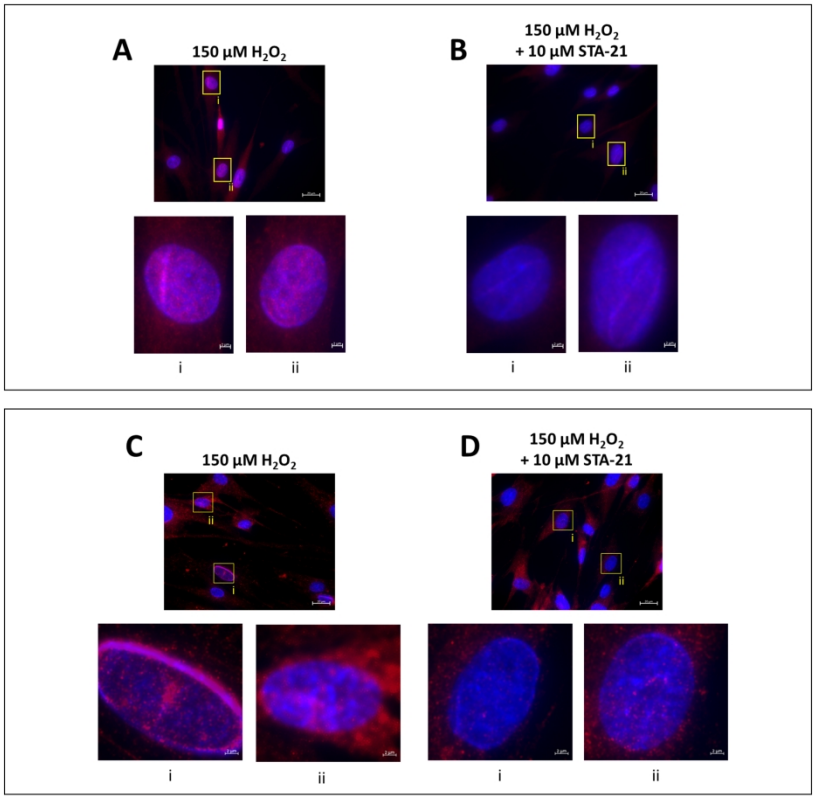

Figure 5. nuclear and mitochondrial localization of STAT3 and pSTAT3705 after STAT3 inhibition. Sub-confluent primary human lung fibroblasts treated with 150µM H2O2 with or without the addition of 10µM STA-21 were grown for 72 hrs. Images A - D show the nuclear localization of STAT3 and pSTAT3705 (red = STAT3/ pSTAT3705, blue = DAPI). Each condition has two nuclei highlighted and enlarged for more accurate assessment of localization (i, ii). Images E-H describe mitochondrial localization of STAT3 and pSTAT3705 (green = mitochondria, red = STAT3/ pSTAT3705, blue = DAPI). Each condition has 3 separate images enlarged to highlight mitochondria only, STAT3/ pSTAT3705 only, and a merged image. Images were taken at 63x magnification under oil immersion (n=3).

338x399mm (300 x 300 DPI)

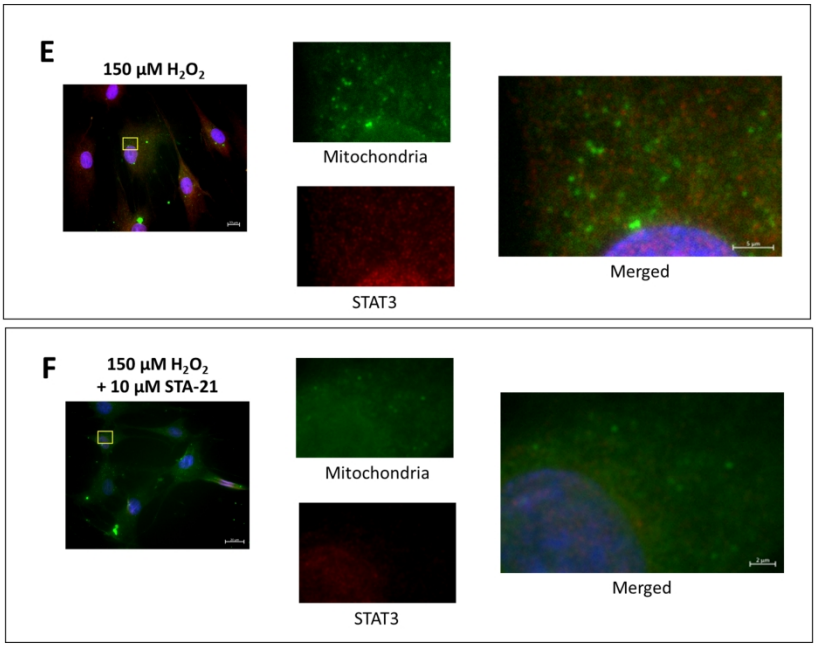

Figure 5. nuclear and mitochondrial localization of STAT3 and pSTAT3705 after STAT3 inhibition. Sub-confluent primary human lung fibroblasts treated with 150µM H2O2 with or without the addition of 10µM STA-21 were grown for 72 hrs. Images A - D show the nuclear localization of STAT3 and pSTAT3705 (red = STAT3/ pSTAT3705, blue = DAPI). Each condition has two nuclei highlighted and enlarged for more accurate assessment of localization (i, ii). Images E-H describe mitochondrial localization of STAT3 and pSTAT3705 (green = mitochondria, red = STAT3/ pSTAT3705, blue = DAPI). Each condition has 3 separate images enlarged to highlight mitochondria only, STAT3/ pSTAT3705 only, and a merged image. Images were taken at 63x magnification under oil immersion (n=3).

338x399mm (300 x 300 DPI)

AJRCMB Articles in Press. Published on 04-January-2019 as 10.1165/rcmb.2018-0328OC

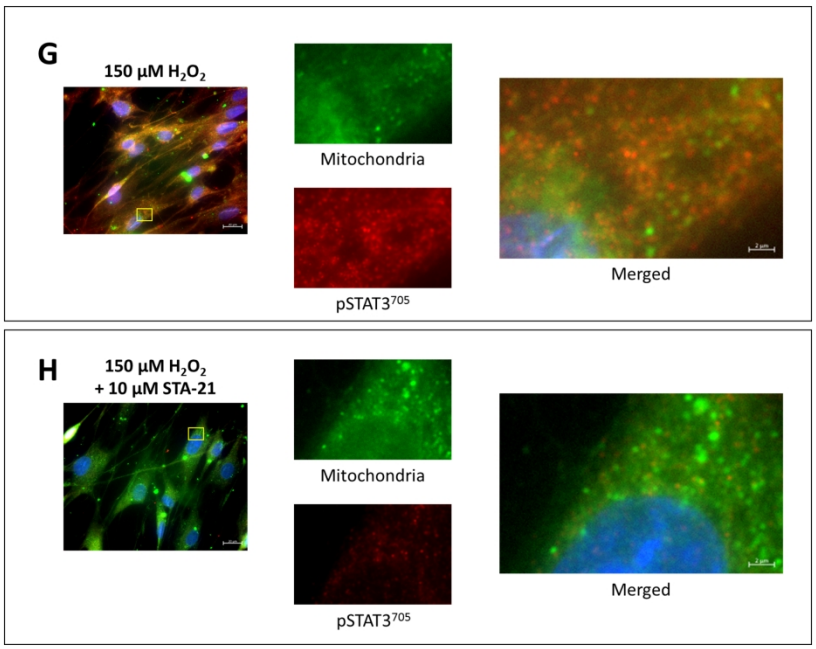

Figure 5. nuclear and mitochondrial localization of STAT3 and pSTAT3705 after STAT3 inhibition. Sub-confluent primary human lung fibroblasts treated with 150µM H2O2 with or without the addition of 10µM STA-21 were grown for 72 hrs. Images A - D show the nuclear localization of STAT3 and pSTAT3705 (red = STAT3/ pSTAT3705, blue = DAPI). Each condition has two nuclei highlighted and enlarged for more accurate assessment of localization (i, ii). Images E-H describe mitochondrial localization of STAT3 and pSTAT3705 (green = mitochondria, red = STAT3/ pSTAT3705, blue = DAPI). Each condition has 3 separate images enlarged to highlight mitochondria only, STAT3/ pSTAT3705 only, and a merged image. Images were taken at 63x magnification under oil immersion (n=3).

338x399mm (300 x 300 DPI)

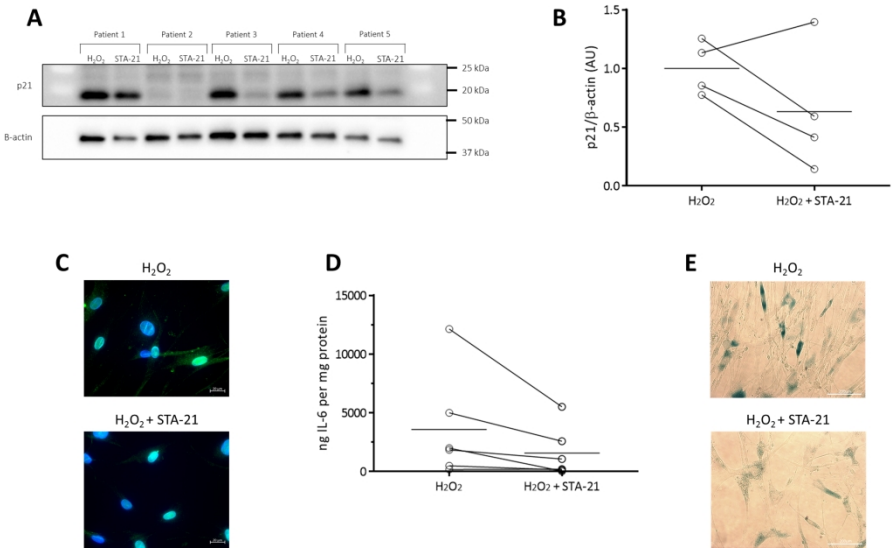

Figure 6. STAT3 inhibition attenuates the shift into senescence. Confluent primary human lung fibroblasts treated with 150μM H2O2 with or without the addition of 10μM STA-21 were grown for 72 hrs. STAT3 inhibition resulted in a reduction of p21, (A) immunoblot analyses of fibroblast cultures treated with H2O2 only and H2O2 + STA-21 (STA-21) (n=5) using specific antibodies against p21, and β-actin as loading control. B) graphed densitometry of a p21 immunoblot after H2O2 only and with the addition of STA-21, (n=4), densitometric analysis of Patient 2 from Figure 6A was not possible due to insufficient resolution of p21 band. C) Immunofluorescence of fibroblasts stained for p21 (blue = DAPI and green = p21). IL-6 production measured in the supernatant by ELISA (D), normalised to mg protein. (n=6). E) SA-β-Gal content (blue = SA-β-Gal). Graphs displays the mean, individual data points were compared between H2O2 and the addition of STA-21 (H2O2 + STA-21) using paired Students t-test (A, B). All images are representative (n=3).

338x190mm (300 x 300 DPI)

AJRCMB Articles in Press. Published on 04-January-2019 as 10.1165/rcmb.2018-0328OC

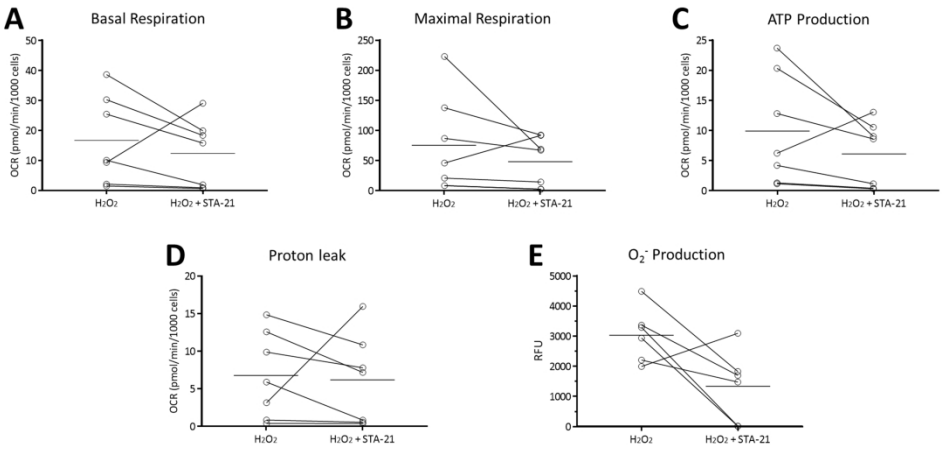

Figure 7. Mitochondrial function is restored after STAT3 inhibition. The mitochondrial functions of basal respiration (Figure 7A), maximal respiration (Figure 7B), ATP production (Figure 7C), and proton leak (Figure 7D) were again assessed using the Mito Stress Test assay (n=7), OCR is reported per 1000 cells. Mitochondrial superoxide production measured using the same fluorogenic dye specific for mitochondrial superoxide as previous (Figure 7E, n=5). All graphs display matched data points compared between fibroblasts treated with H2O2 only and fibroblasts treated with H2O2 and STA-21 2-hrs after H2O2 treatment (H2O2 + STA-21) using paired Students t-test (A-E).

338x190mm (300 x 300 DPI)

Online Supplement

Methods

Cell culture

Lung tissue was minced into ~2mm^3 pieces and allowed to adhere to plastic culture plates for 10-minutes in the absence of media. Tissue samples were then incubated in Dulbecco's Modified Eagle's Medium GlutaMAX Low Glucose (ThermoFisher Scientific) supplemented with HEPES (16mM), 10% Fetal Bovine Serum (v/v), penicillin (50U/ml), streptomycin (50µg/ml), 2.5µg/ml amphotericin B (All from Sigma-Aldrich) and 0.5 µg/ml mycoplasma removing agent (Bio-Rad Laboratories) at 37ºC in air containing 5% CO_2. Cells were grown to confluence over 3-4 weeks, at which point tissue pieces were removed, adherent cells were passaged when culture flask was at 90% confluence. Later passages were maintained in 10% FCS DMEM containing HEPES, penicillin and streptomycin. Experiments were performed with fibroblasts at passage-2 (P2) to P6.

Treatment protocol

Fibroblasts incubated in media containing 0.4% FBS (24 hrs) were exposed to 150µM H_2O_2 (Merck) for 2 hrs. After which point, both treated and non-stimulated control fibroblasts had their media removed, were washed twice with a matching volume of PBS (Gibco) and incubated in media containing 0.4% FBS at 37°C in air containing 5% CO_2 for 72 hrs. To

AJRCMB Articles in Press. Published on 04-January-2019 as 10.1165/rcmb.2018-0328OC

determine the influence of STAT3 in the senescent phenotype the small molecule inhibitor STA-21 (10μM) (Selleckchem) was added once H_2O_2 had been removed, cells had been washed twice in PBS and fresh media had been replenished. All measurements, unless otherwise stated, were obtained 72 hrs after H_2O_2 exposure.

Protein quantification and immunoblot

Mitochondrial fractions were isolated using a Mitochondria Isolation Kit (Thermo Scientific) and lysed with RIPA lysis buffer containing protease (Roche) and phosphatase (Sigma-Aldrich) inhibitors. Fibroblast cultures were lysed with RIPA lysis buffer containing protease (Roche) and phosphatase (Sigma-Aldrich) inhibitors and centrifuged at 14000 x *g* for 15 mins at 4C˚ to separate debris. Protein concentrations were measured using the Pierce BCA protein assay kit (Thermo Scientific). Equal amounts of protein were loaded with 4 x Laemmli Sample Buffer (Bio-Rad) and subjected to SDS polyacrylamide gel electrophoresis (SDS-PAGE) using 4-15% Mini-Protean TGX 10- and 15-well gels (BioRad) and transferred to a nitrocellulose membrane (BioRad) in a semi-dry transfer unit (Hoefer™). Membranes were blocked in a 5% BSA/ 2.5% non-fat milk powder in Tris-buffered saline and 0.5% Tween 20 (TBST) buffer for 1 hour. Membranes were then incubated overnight at 4°C with desired antibodies (Table 1 supplement). Membranes were washed with TBST (3 x 10 mins) and incubated with IgG secondary antibodies conjugated to horseradish peroxidase (HRP) for 1 hour at RT. Secondary antibodies were removed with 3 x 10 mins washes in TBST and membranes were imaged using SuperSignal West Femto Maximum Sensitivity Substrate reagents (ThermoFisher Scientific) on a ChemiDoc MP Imaging System (BioRad). The intensity of bands of interest were quantified using Image Lab version 5.1 (BioRad) and normalised to β-actin for densitometric analysis.

mRNA extraction, quantification and PCR

Total messengerRNA (mRNA) was extracted from cultured fibroblast samples using a RNeasy mini kit (Qiagen) according to the manufacture's instructions and quantified using a nano-drop 2000 spectrophotometer (Thermo Scientific). 200ng mRNA of each sample was used for cDNA synthesis using the high-capacity cDNA reverse transcription kit (Applied Biosystems). Genes of interest were quantified by qPCR using iTaq Universal SYBR Green (Bio-Rad) (Primer information in Table S3). Expression levels were normalized to 18S rRNA and displayed as fold differences relative to non-stimulated.

Immunofluorescence staining

Fibroblasts were fixed with 4% paraformaldehyde for 15 mins and washed in 0.05M glycine/PBS and permeabilized with 0.5% Triton X-100/PBS for 10 min. Non-specific antibody binding was blocked by addition of 10% goat serum/PBS for 1hr at room temperature. Cells were incubated with primary antibodies at 4°C overnight followed by incubation with fluorescently labelled secondary antibodies (Cell Signalling Technology) for 1hr at room temperature. ProLong Gold mountant (Thermo Scientific) with DAPI nuclear stain was used to fix coverslips to slides. Images were visualized using an Axio Imager 2 (Zeiss). Mitochondrial staining was carried out using the MITO-ID detection kit (Enzo Life Sciences) (Antibodies in Table S2).

Assessment of mitochondrial superoxide production by fluorescence intensity

Mitochondrial generated superoxide was detected using the fluorescent MitoSox probe (Invitrogen). Cells were incubated in HBSS (no phenol red, Gibco) containing 2 µM MitoSox-

AJRCMB Articles in Press. Published on 04-January-2019 as 10.1165/rcmb.2018-0328OC

Red for 30 min at 37 °C in a 5% CO_2 atmosphere, washed once with HBSS and fluorescence levels were assessed using a FLUOstar OPTIMA microplate reader (BMG Labtech).

Seahorse respiration assay

Mitochondrial function was assessed using the Agilent Seahorse Mito Stress Test Kit (Seahorse Bioscience) as per the operating system. Ten thousand cells per well were seeded in a 96-well Seahorse plate, samples were plated in replicates of eight. Optimised protocol settings involved using final concentrations of compounds: oligomycin 2 µM, FCCP 1 µM, and rotenone/antimycin A 0.5 µM. Raw values from the assay were normalised to cell counts, each well was stained with DAPI immediately after the Mito Stress Test and cell counts were performed on a IncuCyte 3 S3 Live Cell Analysis System (Sartorius). Oxygen consumption rate (OCR) per 1000 cells are reported.

Results

3.3 STAT3 activity after oxidant induced senescence.

To investigate whether STAT3 activation increased as a consequence of oxidative stress we harvested whole cell lysates at eight time points after H_2O_2 exposure. Densitometric analysis revealed that across the three patients studied STAT3 activity did not consistently increase in those cultures treated with H_2O_2 and did not provide a clear indication of the role of STAT3 activity during oxidant-induced senescence.

Supplement Figure 1. **STAT3 and pSTAT3^{705} expression after H_2O_2 treatment**. Time points after H_2O_2 treatment included 0.5 hrs, 2 hrs, 4 hrs, 8 hrs, 12 hrs, 24 hrs, 48 hrs, and 72 hrs. Three individual lung fibroblast cultures were used to carry out the time course, protein lysates were used to probe for STAT3, and pSTAT3^{705} via immunoblot. A) Representative immunoblot of non-stimulated cultures (NS) and cultures treated with H_2O_2 probed with antibodies against STAT3 and pSTAT3^{705}, β-actin used as a loading control. Graphs represent densitometry of immunoblots for STAT3 and pSTAT3^{705}. Both the STAT3 (B, D, E) and pSTAT3^{705} (C, F, G) content of H_2O_2 treated cultures shows a similar trend to non-stimulated cultures.

AJRCMB Articles in Press. Published on 04-January-2019 as 10.1165/rcmb.2018-0328OC

Tables

Table S1: Characteristics of fibroblast samples.

Fibroblast Sample No.	Age	Sex	Smoking History (Pack yrs)
1	28	F	Former
2	44	F	n/a
3	67	F	N/A
4	61	F	N/A
5	66	F	N/A
6	71	F	N/A
7	69	M	Former (20)
8	70	M	Former (105)
9	79	M	Former (32)
10	68	M	Former (79.5)
11	56	M	N/A
12	39	N/A	Former (15)
13	35	N/A	N/A
14	N/A	N/A	N/A
15	N/A	N/A	N/A

Table S1. Characteristics of fibroblast samples. Characteristics include age, gender, and smoking history (Pack years), N/A = data not available. Mean age of patients 58 years including 6 patients under 65 years, 7 patients over 65 years, 2 patients ages N/A. Fibroblast Sample No. is not representative of nomenclature in figure legends. Samples were chosen at random for any particular assay.

Table S2: Antibodies used.

Antibody	Manufacturer	ID	Application	Concentration
Phospho-STAT3^{705}	ABCAM	#76315	IF	1:50
β-Actin	ABCAM	#8227	WB	1:20,000
p21	BD Biosciences	#556430	WB/ IF	1:1000/ 1:50
Phospho-STAT3^{705}	Cell Signalling	#4113	WB	1:1000
COX-IV	Cell Signalling	#4850	WB	1:1000
Phospho-p53	Cell Signalling	#9284	IF	1:50
STAT3	Cell Signalling	#9139	WB/IF	1:1000/ 1:50

Table S2. Antibodies used throughout the study manufacturer's product number (ID), and application used. WB = Western blot, IF = Immunofluorescence.

Table S3: qPCR primers used.

Gene	Manufacturer	Forward Primer2	Reverse Primer2
18S ribosomal RNA (18S rRNA)	Sigma-Aldrich	ATCGGGGATTGCAATTATTC	CTCACTAAACCATCCAATCG
CCND1 (Cyclin D1)	Sigma-Aldrich	GTGCCACAGATGTGAAG	CTTCGATCTGCTCCTGG
FN1 (Fibronectin-1)	Sigma-Aldrich	TCAGAGATACCATCAGAGAAC	GAAAGAACTCTAAGCTGG

Table S3. qPCR primers.

AJRCMB Articles in Press. Published on 04-January-2019 as 10.1165/rcmb.2018-0328OC

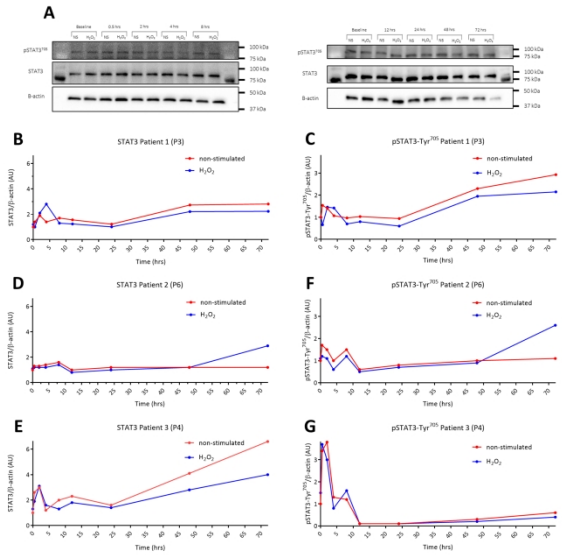

Supplement Figure 1. STAT3 and pSTAT3705 expression after H2O2 treatment. Time points after H2O2 treatment included 0.5 hrs, 2 hrs, 4 hrs, 8 hrs, 12 hrs, 24 hrs, 48 hrs, and 72 hrs. Three individual lung fibroblast cultures were used to carry out the time course, protein lysates were used to probe for STAT3, and pSTAT3705 via immunoblot. A) Representative immunoblot of non-stimulated cultures (NS) and cultures treated with H2O2 probed with antibodies against STAT3 and pSTAT3705, β-actin used as a loading control. Graphs represent densitometry of immunoblots for STAT3 and pSTAT3705. Both the STAT3 (B, D, E) and pSTAT3705 (C, F, G) content of H2O2 treated cultures shows a similar trend to non-stimulated cultures

338x190mm (300 x 300 DPI)